Control Engineering Practice 113 (2021) 104841

Contents lists available at ScienceDirect

Control Engineering Practice

journal homepage: www.elsevier.com/locate/conengprac

Data-driven robust model predictive control framework for stem water potential regulation and irrigation in water management

Wei-Han Chen [a], Chao Shang [b], Siyu Zhu [a], Kathryn Haldeman [a], Michael Santiago [c], Abraham Duncan Stroock [a], Fengqi You [a,*]

[a] Smith School of Chemical and Biomolecular Engineering, Cornell University, Ithaca, NY 14853, USA
[b] Department of Automation, BNRist, Tsinghua University, Beijing 100084, China
[c] FloraPulse Co at 170 Louise Ln, Davis, CA 95618, USA

ARTICLE INFO

Keywords:
Irrigation control
Data-driven robust optimization
Robust model predictive control uncertainty

ABSTRACT

In this work, we propose a data-driven robust model predictive control (DDRMPC) framework that utilizes stem water potential (SWP) as a basis for effective irrigation control of high value-added crops. By linearizing and discretizing a nonlinear dynamic model of water dynamics, we develop a state-space model that predicts the dynamic state of SWP. In the model, soil, root, and stem are the three compartments to describe current water status of the system. In addition, evapotranspiration and precipitation are the driving force and the water inlet, respectively. A robust optimal control problem is formulated to maintain SWP above a safe level to avoid detrimental effects on crops. To describe the uncertainty within prediction errors of evapotranspiration and precipitation, a data-driven approach is adopted, which achieves a desirable tradeoff between constraint satisfaction and water saving. Meanwhile, it is shown that the proposed DDRMPC ensures both feasibility and stability. A case study based on almond tree is carried out to showcase the effectiveness of the DDRMPC strategy relative to on–off control, certainty equivalent MPC and robust MPC. In particular, the control of tree stem water potential through DDRMPC can reduce the water consumption by 7.9% compared with on–off control while maintaining zero probability of constraint violation.

1. Introduction

In the era of increasing water demand caused by population expansion and economic growth, enhancing irrigation efficiency is an important task because 70% of freshwater withdrawals are routinely used for agriculture whereby irrigation consumes the most (United Nations World Water Assessment Programme, 2018). In addition, water supply in some area is also limited because of climate change and drought, thereby further highlighting the importance of irrigation efficiency (Vörösmarty, Green, Salisbury, & Lammers, 2000). In addition to saving valuable water resources, improving irrigation efficiency can increase the production and crop yield. The higher yield per unit of irrigation water, the more profit gained by farmers. Traditional irrigation strategies attempt to maintain soil moisture above a certain level by using open-loop or closed-loop control systems (Romero, Muriel, García, & Muñoz de la Peña, 2012). The open-loop irrigation strategy follows the planned irrigation schedule according to daily weather, soil water-holding capacity, crop species, and the recent irrigated amount. Although such a strategy could be easily implementable, it does not capture the state of soil in real-time. On the other hand, closed-loop irrigation strategies such as on–off control and model predictive control (MPC) adjust the irrigation amount according to the real-time soil status, thus leading to improved irrigation efficiency (Delgoda, Malano, Saleem, & Halgamuge, 2016).

A significant disadvantage of controlling soil moisture is that, growth performance is in fact impacted by stem water potential (SWP) other than the soil moisture level. Although for some plants, there is a relationship between SWP and soil moisture level because water in a tree is absorbed through soil, delay would occur due to the time required for water to move from soil to stem. Soil moisture level could also have a large departure from SWP for some plants that have strong dependence on atmospheric conditions (Mccutchan & Shackel, 1992). Hence, directly controlling SWP would be a better approach to avoid these disadvantages and could make irrigation more efficient, especially for some high value-added plants and crops. In order to collect feedback measurements of SWP for closed-loop control, a sensor like the micro-tensiometer could be implemented inside the stem of a tree, see e.g. Pagay et al. (2014). In this case, a closed-loop control system for controlling SWP is thus of special interest.

MPC is an effective strategy among many feedback control approaches that utilizes prediction of state evolution to optimize future

* Corresponding author.
E-mail address: fengqi.you@cornell.edu (F. You).

https://doi.org/10.1016/j.conengprac.2021.104841
Received 20 November 2020; Received in revised form 26 March 2021; Accepted 6 May 2021
Available online xxxx
0967-0661/

system behavior under certain constraints and has been well adopted in various applications (Gallego, Merello, Berenguel, & Camacho, 2019; Galuppini, Magni, & Raimondo, 2018; Garcia, Prett, & Morari, 1989; Shen, Lim, & Shi, 2020; Weizmann, Görges, & Lin, 2018; Xi, Li, & Lin, 2013). It is also a desirable framework for irrigation control because water potential dynamics is slow and the system model incorporates disturbances and constraints that can be derived from first principles models. Disturbances in irrigation control are mainly related to weather, including precipitation and evapotranspiration. Therefore, weather forecast could serve as a helpful tool to predict disturbances, reduce water consumption and improve irrigation efficiency. There are several studies that demonstrated the advantages of MPC over conventional methods in irrigation control (Delgoda et al., 2016; Romero et al., 2012; Shang, Chen, Stroock, & You, 2019). However, the imperfection of weather forecast might make plants suffer from water stress. For example, when weather forecast indicates an expected heavy rain tomorrow, MPC may choose not to irrigate today to save water. However, it is likely that no rain occurs at all tomorrow. As a consequence, SWP would drop below an acceptable level, leading to a reduced crop yield or poor crop quality. Therefore, uncertainty within weather forecast error is a major challenge for implementing MPC for effective irrigation control.

To tackle the uncertainty of weather forecast errors, robust MPC (RMPC) acts as a viable option (Bemporad & Morari, 1999). This approach first uses a bounded uncertainty set to characterize the support of uncertainty, and then utilizes RMPC to ensure that SWP will not violate the constraints during the control horizon for all weather forecast errors within the uncertainty set. Although RMPC could prevent SWP from dropping significantly, it may lead to over-conservative regulation actions because the geometry of uncertainty set fails to compactly capture the distribution of weather forecast errors. On the other hand, over-conservative control actions are not favorable, since more water consumption is required in this case with reduced efficiency. To reduce the conservatism of RMPC, data-driven robust optimization capturing the high-density region of uncertainties in decision-making has established itself as an effective approach to monitoring, control, and optimization of industrial processes (Shang & You, 2019), and has also been widely adopted in various applications in process operations and control (Gao, Ning, & You, 2019; Kusiak, Li, & Zhang, 2010; Moro, Cortez, & Rita, 2014; Ning & You, 2018a, 2018b, 2019; Pidsley et al., 2013).

Most existing studies on MPC for irrigation control do not consider robustness, given that uncertain disturbances could deviate SWP from the optimal condition (Lozoya, 2014; McCarthy, Hancock, & Raine, 2014; Romero et al., 2012). RMPC was adopted in Delgoda et al. (2016), but the possibility of over-conservatism due to the oversized uncertainty set is not considered. The issue of over-conservatism was addressed in Shang et al. (2019). However, controlling soil moisture level is not as direct as controlling SWP. Thus, to fill the knowledge gap, the goal of this work is to develop a novel RMPC framework for irrigation control that can (a) control SWP to prevent plant from water stress and/or crop damage while balancing between irrigation amount minimization and controlling the constraint violation; (b) effectively hedge against uncertain disturbances from weather forecast errors including precipitation and evapotranspiration errors; and (c) leverage the value of historical weather forecast data to reduce over-conservatism.

In this work, we propose a novel data-driven robust MPC (DDRMPC) framework for controlling SWP that minimizes the water consumption and ensures the constraint on SWP not being violated by uncertainty of disturbances. The state-space model of water dynamics in soil–root–plant system is first formulated to describe the evolution of water potentials in the near future with precipitation and evapotranspiration forecast being considered. The three compartments, soil, root, and stem, describe the water status of the system. Precipitation replenishes water in the soil, which is further absorbed by the root of a tree thereby alleviating water stress. Evapotranspiration is the driving force in soil–root–plant system and could lead to tree water stress when evapotranspiration is too heavy. Soil, root, and stem can hold water and repel water flow in the sense that they can be viewed as "capacitors" or "resistors" in the system. In order to tackle the computation burden caused by the nonlinearity of the water dynamics, the nonlinear state-space model is further linearized and discretized. In addition, to address the infeasibility issue of controlling SWP, constraints on SWP are softened by introducing slack variables. Next, historical weather forecast data and historical weather measurement data are collected for the calculation of weather forecast errors. Data-driven uncertainty sets are then constructed by adopting support vector clustering (SVC) with weighted generalized intersection kernel (WGIK) (Shang, Huang, & You, 2017). The data-driven uncertainty sets can be seamlessly incorporated into RMPC to alleviate over-conservatism and enhance irrigation efficiency. The affine disturbance feedback (ADF) policy (Goulart, Kerrigan, & Maciejowski, 2006) is utilized to provide tractable approximations of the optimization problem in DDRMPC, which can be solved effectively by off-the-shelf solvers. The stability issue of the proposed control scheme is also addressed formally. A case study using real weather data to simulate almond tree water potential in Arbuckle, California, USA, is presented to demonstrate the DDRMPC result comparing with on–off control, certainty equivalence MPC (CEMPC), and RMPC approaches.

The main contributions of this paper are summarized below:

- A novel DDRMPC framework for irrigation control through SWP capable of handling uncertain disturbances of weather forecast errors;
- A formal stability guarantee of the DDRMPC framework for irrigation control;
- A real-world case study utilizing historical weather data to control SWP of an almond tree located in Arbukle, California, USA;
- Comprehensive comparisons among rule-based control, CEMPC, RMPC, and DDRMPC approaches on SWP control.

The paper is organized as follows: Section 2 presents the dynamic model for water potentials of soil–root–plant system and a brief introduction to on–off control. MPC strategies are set up for regulating SWP in Section 3. In Section 4, a simulation of controlling SWP is served as a case study of the proposed control strategies, and the simulation results of different control strategies are discussed. Section 5 summarizes the conclusion.

Notations and Definitions: $\mathbb{N}_{i:j}$ is the set of consecutive nonnegative integers $\{i, \dots, j\}$. The p-norm of a matrix is denoted by $\|\cdot\|_p$. $\otimes$ denotes the Kronecker product operator. The m-dimensional identity matrix is denoted by $\boldsymbol{I}_m$, and $\mathbf{1}_m$ denotes the m-dimensional vector with all elements being ones.

2. Preliminaries

2.1. System description

Measuring the amount of water in a system is useful to understand the current state of that system. The most common way to measure the water status in plant systems is by water potential (Jones, 2013). Water potential is the potential energy of water compared to pure water, of which the water potential is assigned to zero. When a plant encounters water stress, its SWP would be more negative than normal condition. Therefore, SWP is a measure to quantify the water stress of a plant. Most plants obtain water from soil, and the path of water starts from soil and roots to stems. To develop a water dynamic model for soil–root–plant system, water flow passing soil, root, and stem can be modeled in a way analogous to electrical circuits (Jones, 2013). Soil, root, and stem can contain water and resist water flow such that these compartments serve as either "capacitors" or "resistors" in the system. The dynamics of soil water potential can be described by the following

nonlinear ordinary differential equation (ODE) (Bittelli, Campbell, & Tomei, 2015):

$$\frac{d\psi_{soil}}{dt} = \frac{1}{R_{root}(\psi_{soil})C_{soil}(\psi_{soil})}(\psi_{root} - \psi_{soil}) + \frac{IR(t)}{C_{soil}(\psi_{soil})} \tag{1}$$

where ψ_{soil} and ψ_{root} are water potentials of soil and root, respectively. C_{soil} is the "capacitance" of soil, respectively. R_{root} is the "resistance" of root. Both R_{root} and C_{soil} are dependent on ψ_{soil} because their properties are described by certain nonlinear functions (Zhu, 2020). The addition of precipitation and irrigation rate is denoted by IR, which is the water inflow. The soil is treated as a single compartment in the spirit of parsimony to avoid over fitting our data. Additionally, the plant itself, with its roots distributed throughout the volume of soil, tends to maintain uniformity of water potential (Caldwell, Dawson, & Richards, 1998).

The dynamics of root water potential is given by Bittelli et al. (2015)

$$\frac{d\psi_{root}}{dt} = \frac{1}{R_{stem}C_{root}}(\psi_{stem} - \psi_{root}) + \frac{1}{R_{root}(\psi_{soil})C_{root}}(\psi_{soil} - \psi_{root}) \tag{2}$$

where ψ_{stem} is stem water potential. R_{stem} is the "resistance" of stem. C_{root} is the "capacitance" of root.

Finally, the dynamics of stem water potential is described as Bittelli et al. (2015),

$$\frac{d\psi_{stem}}{dt} = \frac{1}{R_{stem}C_{stem}}(\psi_{root} - \psi_{stem}) - \frac{ET(t)}{C_{stem}} \tag{3}$$

where C_{stem} is the "capacitance" of plant stem. The evapotranspiration rate is denoted by ET and can be estimated with the Penman–Monteith equation using weather data (Bittelli et al., 2015). Evapotranspiration, i.e. the sum of evaporation and plant transpiration from the canopy to the atmosphere, is the driving force of the Resistor–Capacitor (RC) circuit-like model, and the evaporation from bare soil or vegetation surrounding the tree of interest is omitted. Basically, the variations of evapotranspiration follow a daily pattern. After sunrise, air temperature and solar radiation increases, and then the plant opens the stomatal valves in its leaves to capture carbon dioxide while losing water vapor to the atmosphere. These and other weather factors (e.g. relative humidity and wind velocity) and plant characteristics (e.g. growing stage and plant type) all make evapotranspiration during the daytime significantly heavier than that at night.

By combining (1)–(3), the ODE model can be represented as,

$$\dot{\boldsymbol{x}} = \boldsymbol{A}(\boldsymbol{x})\boldsymbol{x} + \boldsymbol{B}_u(\boldsymbol{x})u + \boldsymbol{B}_v(\boldsymbol{x})\boldsymbol{v} + \boldsymbol{B}_w(\boldsymbol{x})\boldsymbol{w} \tag{4}$$

where $\boldsymbol{x}$ is the vector of state variables, which consists of water potentials of soil, root, and stem. u is the control input, which is the irrigation rate. $\boldsymbol{v}$ is the vector of deterministic disturbances, which are evapotranspiration rate and precipitation rate. $\boldsymbol{w}$ is the vector of uncertain disturbances, which are forecast errors of evapotranspiration rate and precipitation rate. $\{\boldsymbol{A}(\boldsymbol{x}), \boldsymbol{B}_u(\boldsymbol{x}), \boldsymbol{B}_v(\boldsymbol{x}), \boldsymbol{B}_w(\boldsymbol{x})\}$ are system matrices dependent on water potentials, which involve nonlinearity, because capacitances and resistances are functions of water potentials.

The availability of direct measurement of system states is critical in irrigation control. Soil water potential measurement has been extensively studied in literature and could be realized by many devices (Campbell, 1988). Beyond that, root water potential measurement is more difficult than soil water potential measurement and has attracted less attentions. Nevertheless, root water potential could still be measured by certain techniques such as using screen-caged thermocouple psychrometers (Oosterhuis, 1987). SWP measurement could be realized by using micro-tensiometer or a more conventional way of pressure chamber (Choné, Van Leeuwen, Dubourdieu, & Gaudillère, 2001; Pagay et al., 2014). The probe is installed at approximately one meter above ground in the main stem (trunk) of the tree in this work. However, the height of the device in modest scale plants will not have a significant impact on the measurement of SWP because gravitational potentials are negligible (0.01 MPa for 1 m) relative to the typical potentials generated by transpiration (~1 MPa). In this work, all system states are assumed to be measurable directly thanks to these existing sensors and devices. Therefore, the need to reconstruct current state by building state observers is alleviated.

2.2. On–off control

Most modern irrigation systems use open-loop control by setting up the irrigation at certain time intervals scheduled in advance (Romero et al., 2012). Therefore, there is no feedback on water deficits or surpluses. In contrast, closed-loop systems could collect information on plant water status and make response. The on–off control strategy is one of the simplest closed-loop irrigation control strategies with widespread usage in practice. The on–off control strategy of SWP adjusts irrigation amount once the difference between stem water potential and the minimum acceptable stem water potential $\psi_{\min}$ is detected to be less than a threshold δ. When the condition is satisfied, controller applies a constant amount of water u_{on} to soil; otherwise, there is no irrigation action at all. In this way, a threshold δ serves as a tuning parameter to prevent SWP from dropping below $\psi_{\min}$, where plants are considered to suffer from water stress and the crop growth and quality could be affected. The control law can be expressed as Flügge-Lotz (1953)

$$u_k = \begin{cases} u_{\text{on}}, & \text{if } \psi_{stem,k} - \psi_{\min} \le \delta \\ 0, & \text{if } \psi_{stem,k} - \psi_{\min} > \delta \end{cases} \tag{5}$$

Even though on–off control has been an effective strategy in soil moisture control, there is a significant challenge in controlling SWP due to a large settling-time of plant dynamics. Because there is a significant time delay for water to flow from soil into tree, water potential could still tend to decline at the beginning of irrigation.

3. The proposed DDRMPC method

MPC is a control strategy that optimizes the control objectives over a prediction horizon while respecting the constraints set for state variables and input variables. One of its characteristics is the capability of handling effects of disturbances and of controlling inputs in the near future. After solving the optimization problem for the current state, control inputs for current state will be implemented and the same procedure again will be repeated at the next sampling instance. MPC could be useful in our scenario, because the evapotranspiration rate and the precipitation rate in the near future could be forecasted by collecting sufficient amount of data from the weather station. In addition, the large settling-time issue in on–off control strategy of SWP can be effectively addressed by implementing MPC because the time for water to be absorbed from soil to stem is described implicitly by the prediction of future system states, provided that the prediction horizon is sufficiently long for the time-delay. However, the nonlinearity of the soil–root–plant water dynamic model is an issue for solving the optimization problem that needs to be handled.

3.1. Linearization and discretization of model

Computational efficiency becomes a critical concern when it comes to solving the nonlinear optimization problem in DDRMPC because the system is a nonlinear ODE model. Some studies show that certain types of nonlinear robust optimization problems could be solved by off-the-shelf solvers after reformulations; however, computation burden remains high when the dimension of the uncertainty is high (Leyffer, Menickelly, Munson, Vanaret, & Wild, 2020; Yuan, Li, & Huang, 2018). The high dimensionality of uncertainties in the present study is resulted from the uncertainty of forecast errors considered throughout the entire prediction horizon H. Therefore, the linearization and discretization strategies are adopted in our DDRMPC framework to alleviate the computation burden caused by the nonlinear model and the high-dimensional uncertainties.

To address the nonlinearity issue, we first linearize (4) at the point (x_0, u_0, v_0, w_0) as a pragmatic approach, where x_0 are the initial water potentials. Although an equilibrium point is commonly chosen as the operating point when linearizing a nonlinear system, in this work, uncertainties exist on the right-hand side of (4). Hence, the equilibrium point could not be found. The linearized continuous-time state-space model is given by,

$$\dot{\boldsymbol{x}} = \boldsymbol{A}_c \boldsymbol{x} + \boldsymbol{B}_{u,c} u + \boldsymbol{B}_{v,c} \boldsymbol{v} + \boldsymbol{B}_{w,c} \boldsymbol{w} + \boldsymbol{C}_c \tag{6}$$

where $\{\boldsymbol{A}_c, \boldsymbol{B}_{u,c}, \boldsymbol{B}_{v,c}, \boldsymbol{B}_{w,c}, \boldsymbol{C}_c\}$ are system matrices derived from (4).

The system model is then discretized using the Euler method, which is an inexact discretization scheme. The system model can now be approximately represented by a linearized discrete-time state-space model shown as,

$$\boldsymbol{x}_{k+1} = \boldsymbol{A}_d \boldsymbol{x}_k + \boldsymbol{B}_{u,d} u_k + \boldsymbol{B}_{v,d} \boldsymbol{v}_k + \boldsymbol{B}_{w,d} \boldsymbol{w}_k + \boldsymbol{C}_d \tag{7}$$

where $\boldsymbol{x}_k \in \mathbb{R}^{n_x}$, $u_k \in \mathbb{R}^{n_u}$, $\boldsymbol{v}_k \in \mathbb{R}^{n_v}$, $\boldsymbol{w}_k \in \mathbb{R}^{n_w}$, k is the time index, and $\{\boldsymbol{A}_d, \boldsymbol{B}_{u,d}, \boldsymbol{B}_{v,d}, \boldsymbol{B}_{w,d}, \boldsymbol{C}_d\}$ are system matrices derived from (6) without much difficulties.

The state-space model can then be formulated into the following compact expression given a prediction horizon H:

$$\mathbf{x} = \mathbf{A} x_0 + \mathbf{B_u} \mathbf{u} + \mathbf{B_v} \mathbf{v} + \mathbf{B_w} \mathbf{w} + \mathbf{C} \tag{8}$$

where $\mathbf{x} = \begin{bmatrix} x_1^T & \dots & x_H^T \end{bmatrix}^T$, $\mathbf{u} = \begin{bmatrix} u_0^T & \dots & u_{H-1}^T \end{bmatrix}^T$, $\mathbf{v} = \begin{bmatrix} v_0^T & \dots & v_{H-1}^T \end{bmatrix}^T$, $\mathbf{w} = \begin{bmatrix} w_0^T & \dots & w_{H-1}^T \end{bmatrix}^T$ are vectors for the state-space model in compact form. System matrices in compact form are given by

$$\mathbf{A} = \begin{bmatrix} A_d \\ {A_d}^2 \\ \vdots \\ {A_d}^H \end{bmatrix}, \quad \mathbf{B_u} = \begin{bmatrix} B_{u,d} & 0 & \cdots & 0 \\ A_d B_{u,d} & B_{u,d} & \cdots & 0 \\ \vdots & \vdots & \ddots & \vdots \\ {A_d}^{H-1} B_{u,d} & {A_d}^{H-2} B_{u,d} & \cdots & B_{u,d} \end{bmatrix},$$

$$\mathbf{B_v} = \begin{bmatrix} B_{v,d} & 0 & \cdots & 0 \\ A_d B_{v,d} & B_{v,d} & \cdots & 0 \\ \vdots & \vdots & \ddots & \vdots \\ {A_d}^{H-1} B_{v,d} & {A_d}^{H-2} B_{v,d} & \cdots & B_{v,d} \end{bmatrix}, \tag{9}$$

$$\mathbf{B_w} = \begin{bmatrix} B_{w,d} & 0 & \cdots & 0 \\ A_d B_{w,d} & B_{w,d} & \cdots & 0 \\ \vdots & \vdots & \ddots & \vdots \\ {A_d}^{H-1} B_{w,d} & {A_d}^{H-2} B_{w,d} & \cdots & B_{w,d} \end{bmatrix}, \quad \mathbf{C} = \begin{bmatrix} C_d \\ {C_d}^2 \\ \vdots \\ {C_d}^H \end{bmatrix}$$

The linearized discrete-time state-space model in (8) is now ready to be integrated in the MPC framework as constraints. The compact form of the state-space model would become a convenient expression for system state constraints that appear in the following section.

3.2. CEMPC

CEMPC, which is the simplest MPC strategy, handles disturbances by replacing them by some predicted values and does not explicitly consider uncertainty in the MPC optimization formulation. In our MPC framework for irrigation control, CEMPC simply replaces disturbances by the values of weather forecast. In this way, uncertain disturbances $\boldsymbol{w}$ in the problem, viz. the forecast errors, are neglected. The MPC problem is therefore simplified to a deterministic control problem. Although CEMPC is a suboptimal policy due to the presence of uncertain disturbances, it still finds widespread applications due to its implementation simplicity (Marquis & Broustail, 1988; Perez, Tzeng, & Goodwin, 2000).

The irrigation control goal is to minimize total water consumption. Therefore, the objective function can be intuitively defined as

$$J = \sum_{i=0}^{H-1} u_i \tag{10}$$

where H is the control horizon.

Among three system states (i.e. water potentials of soil, root, and stem), only SWP is controlled as the primary objective. Hence, constraints on system states are that SWP should be above a minimum acceptable water potential $\psi_{\min}$ to prevent water stress for all SWP in a given prediction horizon H. However, sometimes hard constraints could result in infeasible solutions due to disturbances or limitations of control inputs. In this case, introducing a slack variable ϵ allows constraints to be slightly violated in order to get a consistently feasible solution for the optimization problem, but the penalty of the violation should be incorporated in the objective function to minimize the violation (Qin & Badgwell, 2003). In this work, the slack variable is added to soften the constraint on SWP. The slack variable in the objective function is squared to punish harder if SWP violates the constraint more. The state constraints are now defined as

$$\psi_{stem,k} \geq \psi_{\min} - \epsilon, \quad k \in \mathbb{N}_{1:H} \tag{11}$$

where $\psi_{stem,k}$ is SWP at kth time step, $\psi_{\min}$ is the minimum acceptable SWP, and ϵ is the nonnegative slack variable. After softening system state constraints, the objective function (10) becomes

$$J = \sum_{i=0}^{H-1} u_i + \sum_{i=0}^{H} \rho \epsilon_i^2 \tag{12}$$

where ρ is the constraint violation penalty weight balancing between two conflicting objectives. Besides constraints on SWP, constraints on control input should also be considered because there is a limitation for control input. The control input at kth time step is bounded by,

$$0 \leq u_k \leq u_{\max}, \quad k \in \mathbb{N}_{0:H-1} \tag{13}$$

where $u_{\max}$ is the maximum of the irrigation rate when a faucet is at the full-on position, and the minimum is zero. Unlike state system constraints, softening control input constraints is unreasonable because the maximum and minimum of irrigation rate could not be violated. Thus, control input constraints are inevitably hard. Eq. (11) and (13) can then be combined in succinct expressions as

$$\mathbf{G}_x \mathbf{x} \leq \mathbf{g}_x + \boldsymbol{\epsilon}, \mathbf{G}_u \mathbf{u} \leq \mathbf{g}_u, \boldsymbol{\epsilon} \geq 0 \tag{14}$$

where $\mathbf{G}_x = \boldsymbol{I}_H \otimes \begin{bmatrix} -1 & 0 & 0 \end{bmatrix}$ and $\mathbf{g}_x = \mathbf{1}_H \otimes \begin{bmatrix} -\psi_{\min} & 0 & 0 \end{bmatrix}^T$ are coefficient matrix and vector in water potential constraints, $\mathbf{G}_u = \boldsymbol{I}_H \otimes \begin{bmatrix} -1 & 1 \end{bmatrix}^T$ and $\mathbf{g}_u = \mathbf{1}_H \otimes \begin{bmatrix} 0 & u_{\max} \end{bmatrix}^T$ are coefficient matrix and vector in irrigation rate constraints, and $\boldsymbol{\epsilon}$ is the vector of nonnegative slack variables. The deterministic optimization problem of the CEMPC framework is formulated as

$$\begin{aligned} \min_{\mathbf{u}, \boldsymbol{\epsilon}} \quad & J = \sum_{i=0}^{H-1} u_i + \sum_{i=0}^{H} \rho \epsilon_i^2 \\ \text{s.t.} \quad & \mathbf{x} = \mathbf{A} x_0 + \mathbf{B_u} \mathbf{u} + \mathbf{B_v} \mathbf{v} + \mathbf{C} \\ & \mathbf{G}_x \mathbf{x} \leq \mathbf{g}_x + \boldsymbol{\epsilon} \\ & \mathbf{G}_u \mathbf{u} \leq \mathbf{g}_u \\ & \boldsymbol{\epsilon} \geq 0 \end{aligned} \tag{15}$$

After the prediction horizon H is initialized, the procedure of CEMPC framework at each time step k is summarized as follows:

- *Step 1.* Collect the current water potentials x_k.
- *Step 2.* Linearize and discretize state-space model at x_k to obtain the linearized discrete-time state-space model (8).
- *Step 3.* Solve the optimization problem (15) to obtain control input sequence $\mathbf{u}$.
- *Step 4.* Implement the first control input u_0 to the system.

3.3. RMPC

Forecast errors of weather forecast need to be considered and are regarded as uncertain disturbances in our RMPC problem. Forecast

errors in this work consist of precipitation and evapotranspiration, and their distributions can be assumed to be similar within a few years when forecast accuracy does not have large improvement. Hence, the forecast error distributions of a specific year can be captured by the empirical distributions in the previous year. Historical evapotranspiration forecast errors could be calculated by $w_{ET} = \tilde{v}_{ET} - \hat{v}_{ET}$ where $\tilde{v}_{ET}$ is the historical evapotranspiration measurement, and $\hat{v}_{ET}$ is the historical forecast for evapotranspiration. Similarly, historical precipitation forecast errors could be calculated by $w_{PR} = \tilde{v}_{PR} - \hat{v}_{PR}$ where $\tilde{v}_{PR}$ is the historical precipitation measurement, and $\hat{v}_{PR}$ is the historical forecast for precipitation.

RMPC guarantees constraint satisfaction for the worst case of the bounded disturbances (Bemporad & Morari, 1999). Because MPC typically operates in a receding horizon fashion, the sequent control actions are essentially dependent on previous uncertainty, leading to an infinite-dimensional optimization problem. In order to ensure the tractability of the RMPC problem, ADF policy is adopted, and control input u_k is parameterized according to the past disturbances (Goulart et al., 2006). The past disturbance sequence $\mathbf{w}$ could be calculated as the difference between the predicted and actual states at each step. The control inputs are then parameterized as

$$\boldsymbol{\pi}(\mathbf{w}) = \mathbf{h} + \mathbf{M}\mathbf{w} \tag{16}$$

where

$$\mathbf{h} = \begin{bmatrix} h_0 \\ h_1 \\ \vdots \\ h_{H-1} \end{bmatrix}, \ \mathbf{M} = \begin{bmatrix} \mathbf{0} & \mathbf{0} & \cdots & \mathbf{0} \\ M_{1,0} & \mathbf{0} & \cdots & \mathbf{0} \\ \vdots & \vdots & \ddots & \vdots \\ M_{H-1,0} & \cdots & M_{H-1,H-2} & \mathbf{0} \end{bmatrix} \tag{17}$$

become decision variables of the control problem. The lower triangular structure of $\mathbf{M}$ could assure the causality of ADF policy.

The optimization problem in RMPC is shown as follows, which is a "robustified" version of (15):

$$\begin{aligned} \min_{\mathbf{h},\mathbf{M},\boldsymbol{\varepsilon}} \quad & J = \sum_{i=0}^{H-1} h_i + \sum_{i=0}^{H} \rho \varepsilon_i^2 \\ \text{s.t.} \quad & \mathbf{G}_x \left[\mathbf{A}x_0 + \left(\mathbf{B}_\mathbf{u}\mathbf{M} + \mathbf{B}_\mathbf{w}\right)\mathbf{w} + \mathbf{B}_\mathbf{u}\mathbf{h} + \mathbf{B}_\mathbf{v}\mathbf{v} + \mathbf{C}\right] \le \mathbf{g}_x + \boldsymbol{\varepsilon}, \forall \mathbf{w} \in \mathcal{W} \\ & \mathbf{G}_u \left[\mathbf{M}\mathbf{w} + \mathbf{h}\right] \le \mathbf{g}_u, \forall \mathbf{w} \in \mathcal{W} \\ & \boldsymbol{\varepsilon} \ge 0 \end{aligned} \tag{18}$$

which be solved efficiently with the ADF policy adopted. In robust optimization and RMPC, the budgeted uncertainty set has been mostly used (Bertsimas & Sim, 2004),

$$\mathbf{w} \in \mathcal{W} = \left\{\mathbf{w} \,|\, \|\mathbf{w}\|_1 \le \Omega\right\} \tag{19}$$

where Ω is the budget parameter that is used to adjust the conservatism. A larger value of Ω implies a bigger size of the uncertainty set. However, the generic budgeted set cannot accurately capture the uncertainty distribution and is thus prone to over-conservatism (Bertsimas, Gupta, & Kallus, 2018). In the following section, we discuss a more sophisticated strategy for handling uncertainty in RMPC.

3.4. Uncertainty sets formulation based on data-driven approach

The uncertain disturbance $\mathbf{w}$, as an important ingredient in DDRMPC (Bertsimas et al., 2018), can be characterized by an uncertainty set $\mathcal{W}$. There are several data-driven approaches to uncertainty set construction, including SVC with WGIK (Ben-Hur, Horn, Siegelmann, & Vapnik, 2001; Shang et al., 2017), statistical hypothesis tests (Bertsimas et al., 2018), Dirichlet process mixture model (Ning & You, 2017), copula (Zhang, Jin, Feng, & Rong, 2018), principal component analysis with kernel density estimation (Ning & You, 2018a), probability density contours (Zhang et al., 2018), to name just a few. These mentioned approaches can all serve as the uncertainty set basic ingredients for DDRMPC. Furthermore, the resultant uncertainty set is a polytope that can be parameterized as $D = \{\mathbf{w} \,|\, f(\mathbf{w}) \le \theta\}$.

Uncertainty sets of evapotranspiration and precipitation in this work are formed by SVC with WGIK approach. The minimal sphere radius capturing data could be solved by SVC approach, and WGIK proposed in Shang et al. (2017) is implemented when solving the dual form of SVC optimization problem, which is well suited for robust optimization due to its piecewise-linearity. By following similar approaches in Shang et al. (2019) and Chen, Sim, and Sun (2007), uncertainty set for evapotranspiration is formed as

$$\mathbf{w}_{ET} \in D_{\mathbf{w}_{ET}} = \left\{ \mathbf{w}_{ET} \,\middle|\, \sum_{i \in \mathrm{SV}} \alpha_i \left\| \mathbf{Q}_{ET}(\mathbf{w}_{ET} - \mathbf{w}_{ET}{}^{(i)}) \right\|_1 \le \theta \right\} \tag{20}$$

where $\mathbf{Q}_{ET}$ is the weighting matrix obtained from the covariance matrix of $\mathbf{w}_{ET}$. Model parameters $\{\alpha_i\}$ and uncertainty set parameters θ are determined after solving the dual form of SVC using WGIK. Since (20) is a polytope, solving the resultant robust optimization problem could be accomplished without difficulties. The details of constructing uncertainty set with SVC and WGIK is introduced in Appendix.

The formulation of uncertainty set to describe precipitation is slightly different from the previous one because precipitation is always nonnegative. Therefore, precipitation forecast errors have dependency on the precipitation forecast value. For example, when precipitation forecast is 0 mm for the next hour, precipitation forecast error can only be nonnegative. However, when precipitation forecast is 10 mm for the next hour, precipitation forecast error could be -10 mm as the lowest, which represents no rainfall in the end. In addition, the distribution of precipitation forecast errors is asymmetric around zero. To handle asymmetry in robust optimization, the approach in Chen et al. (2007) is adopted. The technique is to decompose the uncertainty into forward deviation $\mathbf{w}_{PR}^{+}$ and backward deviation $\mathbf{w}_{PR}^{-}$, shown as:

$$\mathbf{w}_{PR} = \mathbf{E}\mathbf{w}_{PR}^{+} - \mathbf{F}\mathbf{w}_{PR}^{-}, \tag{21}$$

$$\overline{\mathbf{w}}_{PR} = \mathbf{w}_{PR}^{+} - \mathbf{w}_{PR}^{-} \in D_{\overline{\mathbf{w}}_{PR}}, \ 0 \le \mathbf{w}_{PR}^{+}, \mathbf{w}_{PR}^{-} \le 1 \tag{22}$$

where $\mathbf{E} = \mathrm{diag}\{e_1, \ldots, e_H\}$ and $\mathbf{F} = \mathrm{diag}\{f_1, \ldots, f_H\}$ contain scaling parameters. The difference between $\mathbf{E}$ and $\mathbf{F}$ helps capturing the asymmetry in $\mathbf{w}_{PR}$. $\overline{\mathbf{w}}_{PR}$ can be regarded as the "primitive uncertainty" and is governed by a homogeneous distribution that can be described by an SVC-based uncertainty set:

$$D_{\overline{\mathbf{w}}_{PR}} = \left\{ \overline{\mathbf{w}}_{PR} \,\middle|\, \sum_{i \in \mathrm{SV}} \alpha_i \left\| \mathbf{Q}_{PR}(\overline{\mathbf{w}}_{PR} - \overline{\mathbf{w}}_{PR}{}^{(i)}) \right\|_1 \le \theta \right\} \tag{23}$$

In this way, the SVC-based precipitation uncertainty set can be shown as

$$D_{\mathbf{w}_{PR}} = \left\{ \mathbf{w}_{PR} \,\middle|\, \begin{matrix} \mathbf{w}_{PR} = \mathbf{E}\mathbf{w}_{PR}^{+} - \mathbf{F}\mathbf{w}_{PR}^{-} \\ \mathbf{w}_{PR}^{+} - \mathbf{w}_{PR}^{-} \in D_{\overline{\mathbf{w}}_{PR}}, \ 0 \le \mathbf{w}_{PR}^{+}, \mathbf{w}_{PR}^{-} \le 1 \end{matrix} \right\} \tag{24}$$

3.5. DDRMPC

The optimization problem of DDRMPC is based on the uncertainty set captured by SVC with WGIK discussed in the previous section to reduce over-conservatism. To ensure the tractability of the DDRMPC problem, ADF policy is adopted and the optimization problem is presented as:

$$\begin{aligned} \min_{\mathbf{h},\mathbf{M},\boldsymbol{\varepsilon}} \quad & J = \sum_{i=0}^{H-1} h_i + \sum_{i=0}^{H} \rho \varepsilon_i^2 \\ \text{s.t.} \quad & \mathbf{G}_x \left[\mathbf{A}x_0 + \left(\mathbf{B}_\mathbf{u}\mathbf{M} + \mathbf{B}_\mathbf{w}\right)\mathbf{w} + \mathbf{B}_\mathbf{u}\mathbf{h} + \mathbf{B}_\mathbf{v}\mathbf{v} + \mathbf{C}\right] \le \mathbf{g}_x + \boldsymbol{\varepsilon}, \forall \mathbf{w} \in D_\mathbf{w} \\ & \mathbf{G}_u \left[\mathbf{M}\mathbf{w} + \mathbf{h}\right] \le \mathbf{g}_u, \forall \mathbf{w} \in D_\mathbf{w} \\ & \boldsymbol{\varepsilon} \ge 0 \end{aligned} \tag{25}$$

The optimization problem can now be converted into a convex optimization problem by using the robust counterpart (Gorissen, Yanıkoğlu,

& den Hertog, 2015). The worst-case maximization problem on the SVC-based precipitation uncertainty set is given by,

$$\begin{aligned}\max_{\mathbf{w}_{PR}^{+},\mathbf{w}_{PR}^{-}} \quad & \mathbf{a}^{T}\mathbf{w}_{PR}^{+}+\mathbf{b}^{T}\mathbf{w}_{PR}^{-} \\ \text{s.t.} \quad & \sum_{i\in \mathrm{SV}}\alpha_i\left\|\mathbf{Q}_{PR}(\mathbf{w}_{PR}^{+}-\mathbf{w}_{PR}^{-}-\overline{\mathbf{w}}_{PR}{}^{(i)})\right\|_1\le\theta \\ & 0\le\mathbf{w}_{PR}^{+},\mathbf{w}_{PR}^{-}\le 1\end{aligned} \tag{26}$$

This problem can be reformulated into its dual problem (Shang et al., 2019)

$$\begin{aligned}\min_{\boldsymbol{\mu}_i,\boldsymbol{\lambda}_i,\mathbf{r},\mathbf{s},\eta} \quad & \sum_{i\in \mathrm{SV}}\left(\boldsymbol{\mu}_i-\boldsymbol{\lambda}_i\right)^{\mathrm{T}}\mathbf{Q}_{PR}\overline{\mathbf{w}}_{PR}{}^{(i)}+(\mathbf{r}+\mathbf{s})^{T}\mathbf{1}+\eta\theta \\ \text{s.t.} \quad & \sum_{i\in \mathrm{SV}}\mathbf{Q}_{PR}\left(\boldsymbol{\mu}_i-\boldsymbol{\lambda}_i\right)+\mathbf{r}\ge\mathbf{a} \\ & \sum_{i\in \mathrm{SV}}\mathbf{Q}_{PR}\left(\boldsymbol{\lambda}_i-\boldsymbol{\mu}_i\right)+\mathbf{s}\ge\mathbf{b} \\ & \boldsymbol{\mu}_i+\boldsymbol{\lambda}_i=\eta\cdot\alpha_i\cdot\mathbf{1},\forall i\in \mathrm{SV} \\ & \boldsymbol{\mu}_i,\boldsymbol{\lambda}_i,\mathbf{r},\mathbf{s}\ge\mathbf{0},\eta\ge 0\end{aligned} \tag{27}$$

where $\boldsymbol{\mu}_i$, $\boldsymbol{\lambda}_i$, $\mathbf{r}$, $\mathbf{s}$, η are the Lagrange multipliers. Following the similar line, the worst-case performance in evapotranspiration uncertainty set can also be found from the dual problem. Hence, constraints in (25) can be reconstructed into multiple linear inequalities and equalities. Since the objective function in (25) is convex, one can reformulate the original DDRMPC optimization problem into a convex problem that can be solved by off-the-shelf solvers efficiently.

For hard-constrained MPC, the feasibility cannot be always guaranteed, which means that the controller may drive system states to a region where the optimal control problem has no feasible solutions. Therefore, it is important in practice to guarantee that the control problem remains feasible all the time. Obviously, the optimization problem (25) underlying the proposed soft-constrained DDRMPC is always feasible. When the hard-constrained robust control problem is infeasible, it implies that constraints on system states are not satisfied even when control inputs have been pushed to the limit. The introduction of slack variables always preserves the feasibility of the problem. The feasibility of the second robust constraint is also guaranteed because one could simply choose $\mathbf{M}=\mathbf{0}$ and $\mathbf{h}$ satisfying $\mathbf{G}_u\mathbf{h}\le\mathbf{g}_u$, ensuring the feasibility of the problem. Another issue is the stability of the proposed soft-constrained DDRMPC. The stability is guaranteed for the proposed soft-constrained DDRMPC. However, the proof is technical, so we defer it to Appendix.

Fig. 1 shows the architecture of the DDRMPC framework in the SWP control problem. First, uncertainty sets for forecast errors are constructed offline from the difference between historical weather measurement and historical weather forecast. Next, for each time step k, DDRMPC solves the optimization problem (25) given current water potentials and weather forecast data in prediction horizon H. Afterwards, only the control input in the first time step is implemented to the soil–root–plant system, and this procedure is repeated for each time step, which is also known as receding horizon control (Kwon & Han, 2006; Mattingley, Wang, & Boyd, 2011).

4. Case study on simulated almond tree

4.1. Problem description

In this section, we perform a closed-loop simulation case study based on weather data collected at Arbuckle, California, USA. The simulation time horizon in this case study is two months. For a comprehensive comparison, on–off control, CEMPC, RMPC, and DDRMPC are implemented. The irrigation control goal is to minimize water usage while maintaining the SWP above −15 bar, which is a critical value indicating moderate stress and could stop plant growth for almond trees (Fulton, Grant, Buchner, & Connell, 2014). Hence, the constraint for SWP, $\psi_{\min}$, is set to −15 bar for all control strategies. For the control input constraint, $u_{\max}$ is set as 0.0014 L/s.

In the case study, the threshold δ is set as -12 bar for on–off control, which is the minimum value that can achieve zero violation. This could be determined according to Figs. 2 and 3. Among all thresholds that result in zero violation shown in Fig. 3, on–off control with the threshold δ being -12 bar and the irrigation rate u_{on} at 0.0012 L/s consumes the least cumulative irrigation. These values are therefore chosen as an appropriate threshold and irrigation rate for on–off control to compare with other control strategies.

Fig. 4 shows ET and precipitation rates at Arbuckle, California, USA in March and April 2017. The ET rate has a diurnal dynamic and the maximum ET rates of each day only have slight differences. On the other hand, precipitation does not occur every day. However, when precipitation occurs, the precipitation rate could be much higher than the ET rate values. Fig. 5 compares nonlinear system trajectory with linearized system trajectory under 6 h of sampling time. Although there are some errors between linearized system trajectory and nonlinear system trajectory, the linearized system model could capture the diurnal dynamics of the stem water potential.

A series of values are attempted for budget parameter $\Omega\in\{0,10^{-5},5\times10^{-5},10^{-4}\}$ in RMPC to investigate the tradeoff between robustness and performance. When $\Omega=0$, RMPC provides no allowance for robustness and will be the same as CEMPC. When $\Omega=10^{-4}$, RMPC has zero violation percentage so the value is chosen for RMPC to compare with other control strategies. Similarly, a set of penalty weights $\rho\in\{10^{-6},10^{-5},10^{-4},10^{-3}\}$ are used in DDRMPC, and $\rho=10^{-4}$ gives zero violation percentage for DDRMPC. Since CEMPC, RMPC, and DDRMPC all contain penalty weight in the optimization problems, the same value of penalty weight $\rho=10^{-4}$ is shared over these control strategies such that a fair comparison could be made.

Uncertainty is tackled in this case by collecting both historical weather data and historical weather forecast data from March to June in both 2016 and 2017 from Meteogram Generator (0000). The length of each time step is set as 6 h, which is appropriate because the system is a slow dynamic process. The prediction horizon H has 4 intervals, which means that weather forecast data looking 24-hour ahead are collected. The linearized discrete-time state-space model is adjusted to the sampling time. Uncertainty sets for evapotranspiration and precipitation can be obtained from the data in 2016, which contain 489 data points with 4 intervals for both uncertainty sets. At each instance, the robust control problem is formulated based on the linearized model of the nonlinear dynamical system (8). Evapotranspiration rate ET is estimated by the simple model in Hargreaves and Samani (1985)

$$ET=0.00023\cdot K_c\cdot RA\cdot TD^{0.5}(T+17.8) \tag{28}$$

where K_c is an evapotranspiration coefficient that Alta fescue grass is taken as reference crop (Hargreaves & Samani, 1985). RA is the extraterrestrial solar radiation. TD stands for annual average daily temperature difference. T is the mean temperature in degree Celsius. To calculate RA for every 6 h, the distribution of solar radiation in each day can be estimated according to latitude and the day of the year (Guo, 2017). By taking reference evapotranspiration and almond tree evapotranspiration coefficient from Allen (1998), the almond tree evapotranspiration amount can be estimated. This estimation model is merely a simple example to estimate evapotranspiration by using temperature and extraterrestrial solar radiation. Indeed, other factors such as wind speed, relative humidity, and cloud cover could be further utilized to enhance prediction accuracy (Cai, Liu, Lei, & Pereira, 2007; Glenn, Huete, Nagler, Hirschboeck, & Brown, 2007; Sumner & Jacobs, 2005). The control problems in the case study are solved by YALMIP toolbox (Lofberg, 2004). Table 1 reports the computational complexities of solving optimization problems in CEMPC, RMPC, and DDRMPC. DDRMPC is significantly more complicated than CEMPC and RMPC because of the Lagrange multipliers introduced to transform the infinite-dimensional problem into its robust counterpart. Nevertheless, the DDRMPC optimization problem could still be calculated rapidly due to constraints and inequalities being all linear.

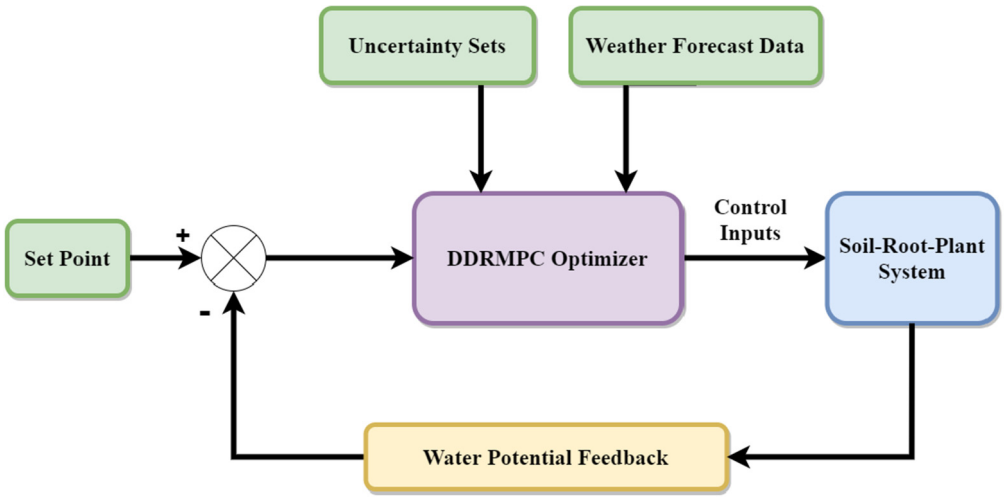

Fig. 1. DDRMPC structure for controlling stem water potential control.

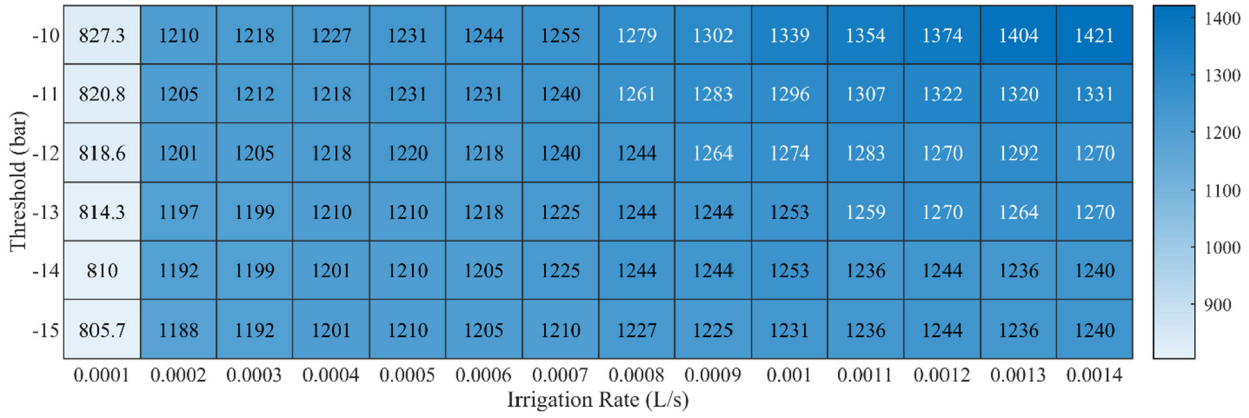

Fig. 2. Heat map of cumulative irrigation amount (L) with different thresholds and irrigation rates in on–off control.

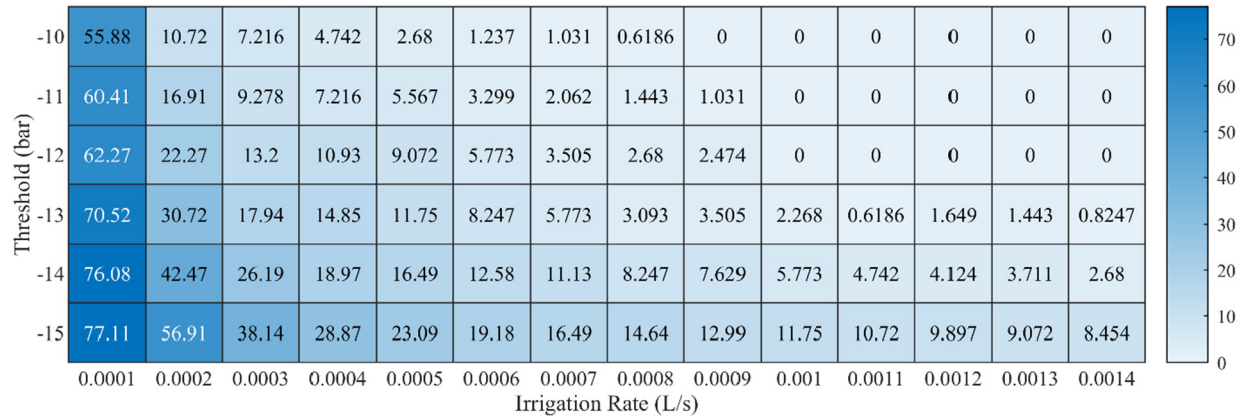

Fig. 3. Heat map of violation percentage (%) with different thresholds and irrigation rates in on–off control.

4.2. Performance criteria

Total water consumption is an important criterion to evaluate the control performance. Besides water usage, the length of total time when the water potential constraint is violated may also cause concerns for the health and productivity of trees. Crops might not grow well or may even be damaged if SWP is below −15 bar. To evaluate this deviation quantitatively, we calculate the percentage of time that SWP drops under −15 bar. We note that the time frequency of water potential constraint violation could not accurately reveal the severity of poor control performance. Even when the SWP is below −15 bar for the same length of time, the water potential that is even more negative will be more harmful to the tree. Therefore, the third performance criterion we consider is the integral of deviation in water potential over time, which is the area below the constraint. Similar to thermal comfort violation in the building climate control presented in Sturzenegger, Gyalistras, Morari, and Smith (2016), SWP violation amount is calculated as the

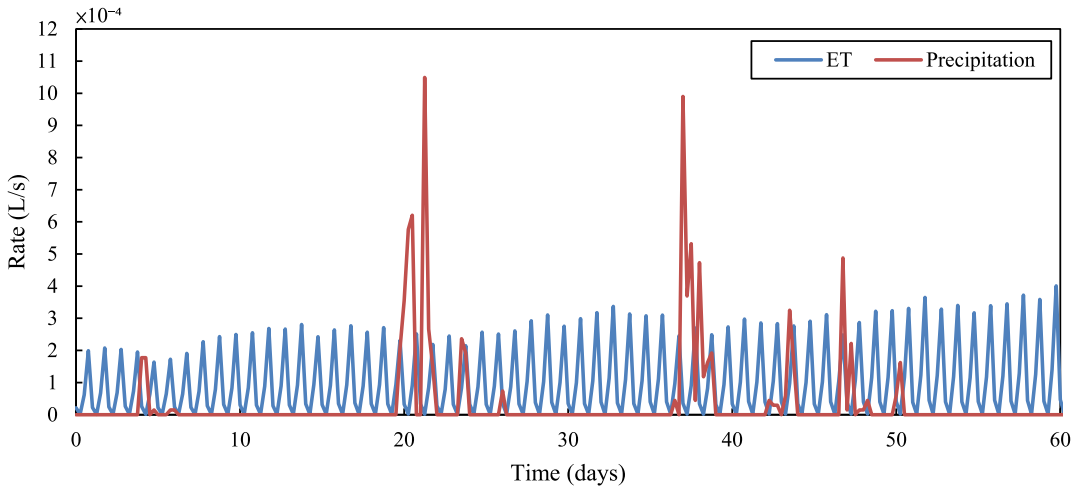

Fig. 4. ET and precipitation rates at Arbuckle, California, USA in March and April 2017.

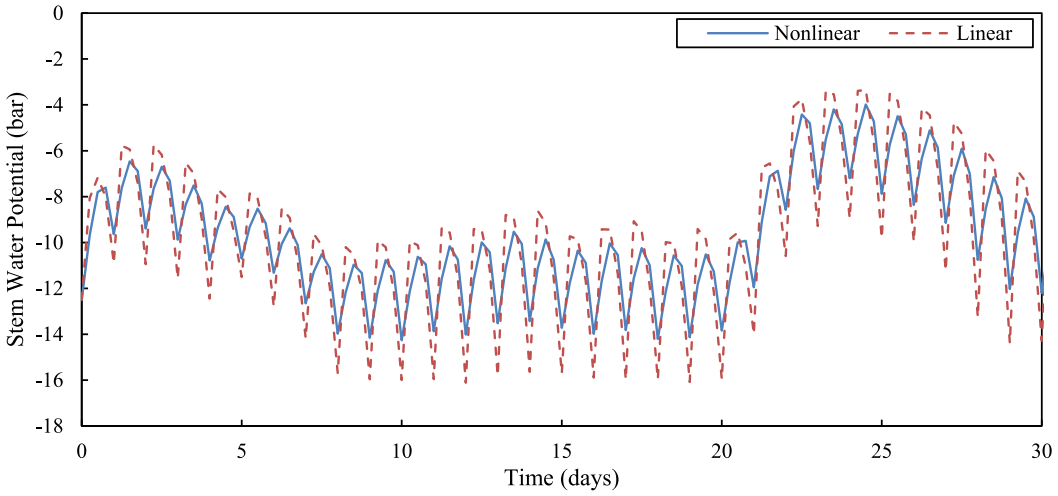

Fig. 5. Comparison of nonlinear system trajectory and linearized system trajectory under 6 h of sampling time.

Table 1
Comparison of computational performance between CEMPC, RMPC, and DDRMPC in terms of number of variables, number of constraints, and average CPU time.

Criteria	Control strategies		
	CEMPC	RMPC	DDRMPC
Number of variables	17	53	2197
Number of constraints	21	77	2949
Average CPU time (s)	0.19	0.21	0.58

area below −15 bar, which is described by

$$\sum_k \max(x_{\min} - x_k, 0) \tag{29}$$

There are more criteria that can be considered to evaluate the performance such as crop qualities or amount of runoff flow, but some might require professional knowledge in plant biology and is beyond the scope of this paper.

4.3. Results and discussion

Fig. 6 shows both daily irrigation amount and cumulative irrigation amount for on–off control, RMPC, and DDRMPC. We note that there is a significant difference of daily irrigation amount between the three control strategies. For instance, RMPC is the only control strategy that irrigates on day 28, but it does not irrigate on day 18 when the two other strategies choose to irrigate. Despite the differences of daily irrigation decisions between on–off control, RMPC, and DDRMPC, cumulative irrigation amounts of the three control strategies are rather similar. Note that DDRMPC consumes the least amount of water while on–off control irrigates the most. The result confirms the advantage of utilizing data of weather forecast errors to improve irrigation efficiency. Furthermore, the fact that RMPC consumes more irrigation amount than DDRMPC indicates that DDRMPC could successfully alleviate over-conservatism.

Figs. 7 and 8 present the water potential dynamic profiles of each control strategy in March and April 2017. The performance of CEMPC and DDRMPC approach the limit of mild stress, which is −15 bar. When SWP stays below −15 bar, an almond tree is under moderate stress and plant growth may stop. However, SWP controlled by CEMPC violates the constraint occasionally, while DDRMPC does not violate it at all. This is because CEMPC neglects weather forecast errors; when weather forecast error is significant (e.g., less precipitation than forecasted or larger evapotranspiration than forecasted), SWP under CEMPC would drop below −15 bar and could be harmful to almond tree growth and almond yield. Figs. 7 and 8 also show that on–off control fluctuates more intensively than the other three strategies. This characteristic is mainly due to the inflexibility of on–off control, which could only

Table 2
Comparison of performance results between on–off control, CEMPC, SP Tracking MPC, RMPC, and DDRMPC in terms of cumulative irrigation amount, violation percentage, and violation amount.

Criteria	Control strategies				
	On–off	CEMPC	SP Tracking MPC	RMPC	DDRMPC
Cumulative irrigation amount (L)	404.3	349.4	385.5	387.2	372.1
Violation percentage (%)	0	14.5	0	0	0
Violation amount (bar-h)	0	249.5	0	0	0

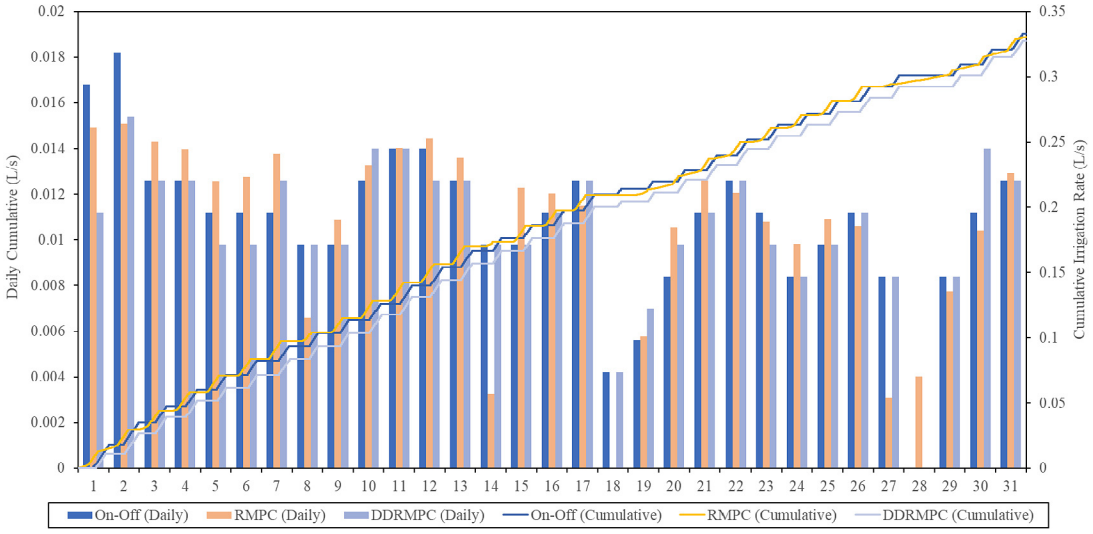

Fig. 6. Daily and cumulative irrigation amount results in March under on–off control, RMPC, and DDRMPC.

irrigate at a constant rate, 0.0012 L/s, or does not irrigate for the entire time step. Therefore, overshooting is more likely to occur when on–off control is implemented. Another factor is that on–off control in this work does not utilize weather forecast. As a result, it is possible that when SWP drops to the threshold for on–off controller to trigger the irrigation action, it starts to rain, which leads to unnecessary water application. As shown in Figs. 7 and 8, control profiles of RMPC and DDRMPC show similar trends and no constraint violation occurs for both strategies. The major difference is that the control profile of DDRMPC is much closer to the limit, −15 bar. This result shows that the data-driven uncertainty sets play a crucial role in reducing conservatism while maintaining zero constraint violation.

Table 2 reports the irrigation control results of on–off control, CEMPC, set-point (SP) tracking MPC, RMPC, and DDRMPC in terms of three performance criteria. SP tracking MPC, which is similar to CEMPC but with a carefully tuned set-point, is included to provide a further comparison. The SP is chosen as −13.5 bar to achieve zero violation percentage. All control strategies except CEMPC achieve zero constraint violation. Among four control strategies without constraint violations, DDRMPC consumes the least amount of water, while on–off control consumes the most irrigation amount. The reason is that DDRMPC integrates weather forecast data and information into controller design, but on–off control does not account for any weather forecast information. On the other hand, CEMPC makes good use of the weather forecast such that it could save water if a rain would be expected in the near future. However, CEMPC leads to some constraint violations because errors always exist in weather forecast. Although SP tracking MPC has zero violation percentage, it still consumes more water than DDRMPC. In addition, SP requires a careful tuning in order to achieve zero constraint violation.

The advantages of DDRMPC are demonstrated through these comparisons. DDRMPC consumes the least amount of water among those control strategies with zero constraint violation. In addition, DDRMPC does not need as much tuning as on–off control to achieve zero violation. Hence, DDRMPC could exploit the data and lead to a desirable balance between saving water and avoiding water potential violation.

5. Conclusion

In this work, we proposed a DDRMPC framework that could effectively control SWP under the uncertainty of weather forecast errors. Instead of controlling soil moisture level, irrigation control based on the water potential inside a tree became a possible method. A state-space model that could capture water dynamics in soil–root–plant system was first formulated. Soil, root, and stem were the three compartments to describe water status of the system. Precipitation in the system was the water inflow, and evapotranspiration was the driving force in the system. Soil, root, and stem also served as "capacitors" or "resistors" in the system. Next, the state-space model was linearized to reduce computation burden caused by nonlinear robust optimization. To avoid SWP from dropping to the level indicating moderate water stress for a plant, a robust optimal control problem was formulated. SVC approach with WGIK was adopted to describe the uncertainty within evapotranspiration and precipitation forecast errors. Optimal irrigation decisions balancing between irrigation amount and constraint satisfaction could then be determined by solving the DDRMPC optimization problem at each time step. The stability issue was also formally addressed. From the simulation results of the case study on almond trees, it was shown that the proposed DDRMPC framework followed the diurnal evapotranspiration pattern, and that DDRMPC outperformed on–off control, CEMPC, and RMPC due to its ability to capture uncertainties in weather forecast errors. Although system states could be measured directly in this work, a state observer is required in general process control settings in the absence system states measurements. The stability of the DDRMPC scheme in the presence of state observer will

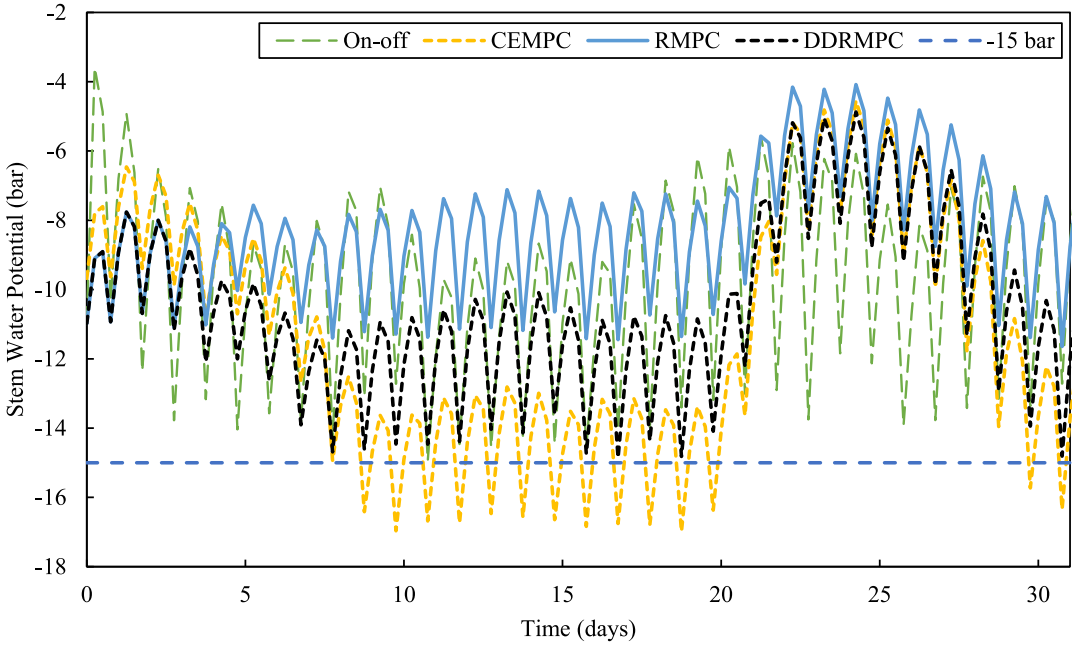

Fig. 7. Stem water potential dynamic profiles in March under on–off control, CEMPC, RMPC, and DDRMPC.

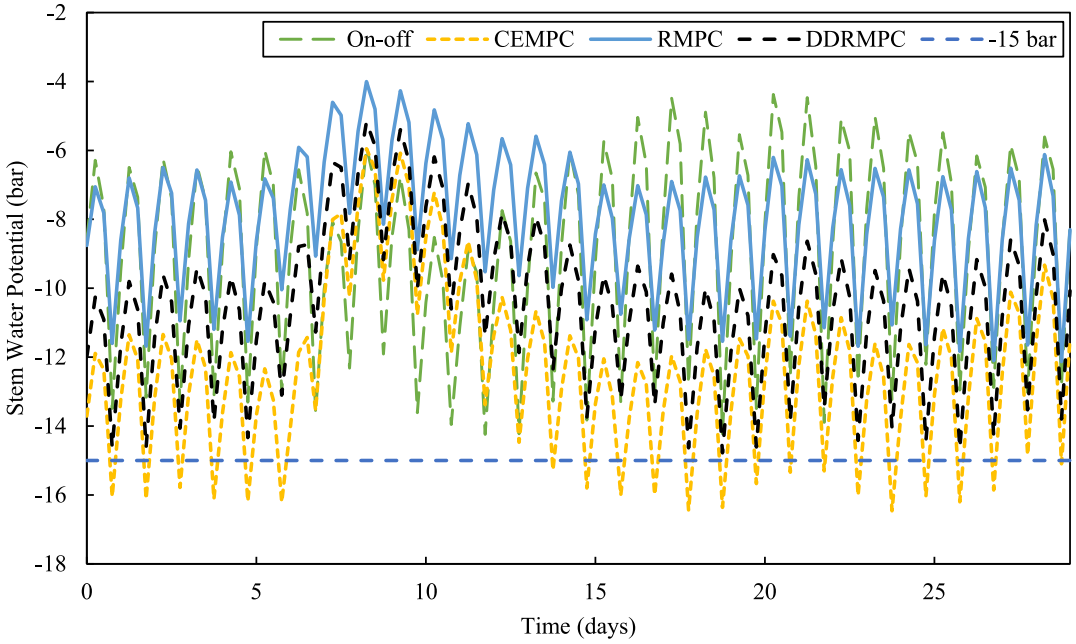

Fig. 8. Stem water potential dynamic profiles in April under on–off control, CEMPC, RMPC, and DDRMPC.

be further investigated in future work. Another potential limitation of the proposed approach is that the current work only focuses on controlling the SWP of a single tree. However, when the SWP of more trees needs to be controlled on a farm, the soil water potential of each tree would be different. This limitation would also be further investigated in future work. Lastly, the DDRMPC framework in this work adopted a linearized model. A nonlinear DDRMPC framework, which could deal with nonlinear models, remains an unsolved research challenge and would be subject to future work.

Nomenclature

$\mathbf{A}$	System matrix of system states in compact form
$\mathbf{B_u}$	System matrix of control inputs in compact form
$\mathbf{B_v}$	System matrix of deterministic disturbances in compact form
$\mathbf{B_w}$	System matrix of uncertain disturbances in compact form
$\mathbf{C}$	System matrix of values derived from Euler's method in compact form

C_{root} Root capacitance

C_{soil} Soil capacitance

$\boldsymbol{E}$ Diagonal matrix containing scaling parameters for forward deviation

ET Evapotranspiration rate

$\boldsymbol{F}$ Diagonal matrix containing scaling parameters for backward deviation

$\mathbf{G}_x$ Coefficient matrix for water potential constraints in compact form

$\mathbf{G}_u$ Coefficient matrix for irrigation rate constraints in compact form

$\mathbf{g}_x$ Coefficient vector for water potential constraints in compact form

$\mathbf{g}_u$ Coefficient vector for irrigation rate constraints in compact form

H Prediction horizon

$\mathbf{h}$ Vector of decision variables for parameterizing u

IR Irrigation rate

k Index of time steps

$\mathbf{M}$ Matrix of decision variables for parameterizing u

$\mathbf{Q}$ Weighting matrix for weighted generalized intersection kernel

R_{root} Root resistance

R_{stem} Stem resistance

$\mathbf{u}$ Control inputs in compact form

u Control inputs

$u_{\max}$ Irrigation rate when faucet at full-on position

u_{on} Irrigation rate when on–off control at "on" position

$\mathbf{v}$ Deterministic disturbances in compact form

v Deterministic disturbances

$\tilde{v}_{ET}$ Historical evapotranspiration measurement

$\tilde{v}_{PR}$ Historical precipitation measurement

$\hat{v}_{ET}$ Historical evapotranspiration forecast

$\hat{v}_{PR}$ Historical precipitation forecast

$\mathcal{W}$ Uncertainty set

$\mathbf{w}$ Uncertain disturbances in compact form

w Uncertain disturbances

$\mathbf{x}$ System states in compact form

x System states

$x_{\min}$ Minimum value acceptable for system states

α Lagrange multipliers for support vector clustering dual problem

δ Threshold in on–off control

ε Slack variable

θ Support vector clustering parameters

$\psi_{\min}$ Minimum value acceptable for stem water potential

ψ_{root} Root water potential

ψ_{soil} Soil water potential

ψ_{stem} Stem water potential

Declaration of competing interest

The authors declare that they have no known competing financial interests or personal relationships that could have appeared to influence the work reported in this paper.

Acknowledgments

The authors would like to thank the editor and all the reviewers for their valuable and constructive comments, which help improve this paper.

Appendix A. Support vector clustering with weighted generalized intersection kernel

SVC is an unsupervised kernel learning approach that finds a sphere with minimal radius to capture the majority of data samples. A nonlinear mapping function $\boldsymbol{\phi}(\mathbf{w})$ is used to map data samples $\mathbf{w}$ from a set D to a high-dimensional features space. The optimization problem to find the sphere is shown as:

$$\begin{aligned} \min_{\mathbf{c},R,\xi} \quad & R^2 + \frac{1}{N\upsilon}\sum_{i=1}^{N}\xi_i \\ \text{s.t.} \quad & \left\|\boldsymbol{\phi}(\mathbf{w}^i) - \mathbf{c}\right\|^2 \le R^2 + \xi_i, i = 1, \dots, N \\ & \xi_i \ge 0, i = 1, \dots, N \end{aligned} \tag{30}$$

where $\mathbf{c}$ is the center point of the sphere, R is the radius of the sphere, and $\{\xi_i\}$ are slack variables. Slack variables are introduced here to allow some outliers not to be enclosed by the sphere. The violations of the outliers are penalized in objective function, and the level of penalization can be adjusted by the regularization parameter υ. The dual problem of (30) is shown as:

$$\begin{aligned} \min_{\boldsymbol{\alpha}} \quad & \sum_{i=1}^{N}\sum_{j=1}^{N}\alpha_i\alpha_j K(\mathbf{w}^{(i)}, \mathbf{w}^{(j)}) - \sum_{i=1}^{N}\alpha_i K(\mathbf{w}^{(i)}, \mathbf{w}^{(j)}) \\ \text{s.t.} \quad & 0 \le \alpha_i \le 1/N\upsilon, i = 1, \dots, N \\ & \sum_{i=1}^{N}\alpha_i = 1 \end{aligned} \tag{31}$$

where $\boldsymbol{\alpha}$ are Lagrange multipliers, and $K\left(\mathbf{w}^{(i)}, \mathbf{w}^{(j)}\right) = \boldsymbol{\phi}(\mathbf{w}^{(i)})^T\boldsymbol{\phi}(\mathbf{w}^{(i)})$ is the kernel function. All data samples can be classified into interior points, boundary points, and outliers according to their locations. If a data sample is an interior point, $\alpha_i = 0$. For boundary points, $0 < \alpha_i < 1/N\upsilon$. Outliers would have $\alpha_i = 1$. The index set of support vectors, which are boundary points and outliers, can be defined as

$$\text{SV} = \left\{i | \alpha_i > 0, 1 \le i \le N\right\} \tag{32}$$

and the index set of boundary points is shown as

$$\text{BSV} = \left\{i | 0 < \alpha_i < 1, 1 \le i \le N\right\} \tag{33}$$

Some common kernel functions such as radial basis function kernel and polynomial kernel contain nonlinear terms and robust optimization problems that incorporates the uncertainty set would become

intractable. To tackle the intractability issue, weighted generalized intersection kernel (WGIK) can be adopted (Shang et al., 2017):

$$K(\mathbf{w},\mathbf{v}) = L - \|\mathbf{Q}(\mathbf{w}-\mathbf{v})\|_1 \tag{34}$$

where matrix $\mathbf{Q} = \boldsymbol{\Sigma}^{-\frac{1}{2}}$ and Σ is the covariance matrix of $\mathbf{w}$. Another kernel parameter L does not affect the solution $\{\alpha_i\}$ as long as it is sufficiently large and could be determined by $\mathbf{w}$ as well.

The data-driven uncertainty set using WGIK can be presented as a polytope

$$\mathcal{W}(v,\mathcal{D}) = \left\{ \mathbf{w} \middle| \sum_{i\in \mathrm{SV}} \alpha_i \left\| \mathbf{Q}(\mathbf{w}-\mathbf{w}^{(i)}) \right\|_1 \le \theta \right\} \tag{35}$$

where

$$\theta = \sum_{i\in \mathrm{SV}} \alpha_i \left\| \mathbf{Q}(\mathbf{w}^{(i')}-\mathbf{w}^{(i)}) \right\|_1, \ i' \in \mathrm{BSV} \tag{36}$$

and $\mathcal{W}(v,\mathcal{D})$ can be further expressed as a series of linear inequalities

$$\mathcal{W}(v,\mathcal{D}) = \left\{ w \middle| \begin{array}{l} \exists \mathbf{v}_i \ \ 1 \le i \le N \\ \text{s.t.} \ \ \sum_{i\in \mathrm{SV}} \alpha_i \mathbf{1}^T \mathbf{v}_i \le \theta, \\ \qquad -\mathbf{v}_i \le \mathbf{Q}(\mathbf{w}-\mathbf{w}^{(i)}) \le \mathbf{v}_i, \ \ 1 \le i \le N \end{array} \right\} \tag{37}$$

where $\{\mathbf{v}_i\}_{i=1}^N$ are auxiliary variables introduced to eliminate 1-norm functions. The main advantage of the introduced data-driven uncertainty is that it is a polytope so the tractability of robust optimization problem can be assured with (37).

Appendix B. Stability guarantee

The stability of the proposed soft-constrained DDRMPC is an issue. It is known that the stability of stochastic system (6) relies on the system matrix $\boldsymbol{A}$. When $\boldsymbol{A}$ is Schur-stable, the mean-square stability $\sup_{k\in\mathbb{N}_0} \mathbb{E}\left\{ \|x_k\|^2 \right\} < \infty$ can be ensured with bounded inputs and bounded covariance of $\mathbf{w}$ (Paulson, Buehler, Braatz, & Mesbah, 2020). If there is at least one eigenvalue of $\boldsymbol{A}$ outside the unit circle, then the mean-square stability cannot be ensured. The only case that needs to be tackled is a Lyapunov stable matrix $\boldsymbol{A}$. In this case, it suffices to consider an orthogonal $\boldsymbol{A}$, i.e. $\boldsymbol{A}^{\mathrm{T}}\boldsymbol{A} = \boldsymbol{I}$ (Chatterjee, Hokayem, & Lygeros, 2011). Towards this goal, we first define X^{nom} as the set of initially feasible states for nominal DDRMPC problem,

$X^{\mathrm{nom}} = \{x_0 | \exists \mathbf{h}$ such that (24) is feasible and $\epsilon = 0\}$.

Some standing assumptions are then made as follows.

Assumption 1. The stochastic process $\{w_k\}_{k\in\mathbb{N}_0}$ satisfies

$$\sup \mathbb{E}\left\{ \|w_k\|^4 \right\} = C_4 < \infty \tag{38}$$

Assumption 2. For the maximal control input $u_{\max}$ in DDRMPC controller, there exists a constant $r > \|B_w\|_2 \cdot \sup_{k\in\mathbb{N}_0} \mathbb{E}\{\|w_k\|\}$ such that

$$\|Ax_k + B_u u_{\max}\| - \|x_k\| \le -r, \ \forall x_k \notin X^{\mathrm{nom}} \tag{39}$$

Notice that different from generic robust control techniques, we do not place a bounded assumption upon w_k. This is because w_k represents the prediction error, which depends on a particular prediction model and is likely to be excessively large. Rather, Assumption 1 requires that the fourth moment of $\{w_k\}_{k\in\mathbb{N}_0}$ is finite, which is not restrictive. Assumption 2 postulates that the controller is capable of steering the nominal system states towards origin. This can be interpreted as the improvement, as measured by r, must overcome the disturbance effect by exceeding the largest expectation of $\|B_w\|_2 \cdot \|w_k\|$. The constraint in Assumption 2 is not required to be satisfied throughout the whole time, but it must be satisfied when $\|x_k\|$ is large and the problem in (25) without soft-constraints is infeasible.

Lemma 1 (*Pemantle & Rosenthal, 1999*). *Assume $\{\eta_k\}_{k\in\mathbb{N}_0}$ is a sequence of random variables upper bounded by $\eta_{\max}$, and let $\{\zeta_k\}_{k\in\mathbb{N}_0} = \{\eta_{\max} - \eta_k\}_{k\in\mathbb{N}_0}$, which is a sequence of nonnegative random variables on some probability space $(\Delta, \mathcal{F}, \mathbb{P})$ and can be regarded as a stochastic process. Let $\{\mathcal{F}_k\}_{k\in\mathbb{N}_0}$ be any filtration to which $\{\zeta_k\}_{k\in\mathbb{N}_0}$ is adapted. Suppose that there exist constants $b > 0$, and $Z, M < \infty$, such that $\zeta_0 < Z$, and for all k,*

$$\mathbb{E}\{\zeta_{k+1} - \zeta_k | \mathcal{F}_k\} \le -b \text{ on the event } \{\zeta_k > Z\}, \text{ and} \tag{40}$$

$$\mathbb{E}\left\{ |\zeta_{k+1} - \zeta_k|^4 | \zeta_0, \ldots, \zeta_k \right\} \le M \tag{41}$$

Then there exists a constant $\gamma = \gamma(b, Z, M) > 0$ such that $\sup_{k\in\mathbb{N}_0} \mathbb{E}\{\zeta_k^2\} < \gamma$.

Details of the proof can be found in Pemantle and Rosenthal (1999) and are omitted here. Now we are ready to establish the stability guarantee.

Theorem 1 (*Mean-Square Stability*). *Suppose that admissible control inputs are bounded $\sup_{h\in F_u} \|h\| = r_h < \infty$, and Assumptions 1 and 2 are satisfied, then for all initial states x_0 there always exists a constant $\gamma > 0$ such that the closed-loop system admits the mean-square boundedness:*

$$\sup_{k\in\mathbb{N}_0} \mathbb{E}\left\{ \|x_k\|^2 \right\} = \gamma < \infty \tag{42}$$

Proof. The condition (40) is to be verified first. A non-negative stochastic process is defined as $\{\zeta_k = \|x_k\|\}_{k\in\mathbb{N}_0}$. Since X_H^{nom} is bounded, we set $Z = \sup_{x\in \mathrm{X}^{\mathrm{nom}}} \|x\| < \infty$. On the event $\zeta_k \ge Z$, we have

$$\begin{aligned} &\mathsf{E}\{\zeta_{k+1} - \zeta_k | \mathsf{F}_k\} \\ &= \mathsf{E}\{\|Ax_k + B_u u_{\max} + B_w w_k\| - \|x_k\| \,|\mathsf{F}_k\} \\ &\le \mathsf{E}\{\|Ax_k + B_u u_{\max}\| + \|B_w w_k\| - \|x_k\| \,|\mathsf{F}_k\} \\ &\le -r + \mathsf{E}\{\|B_w w_k\| \,|\mathsf{F}_k\} \\ &\le -r + \|B_w\|_2 \cdot \sup_{\|w_k\|} \mathsf{E}\{\|w_k\|\} \end{aligned} \tag{43}$$

$$\begin{aligned} y_{k+1} &= (A^T)^{k+1} x_{k+1} \\ &= (A^T)^t x_k + (A^T)^{k+1} [B_u u_{\max} + B_w w_k] \\ &= y_k + (A^T)^{k+1} [B_u u_{\max} + B_w w_k] \end{aligned} \tag{44}$$

Meanwhile, because $\|y_k\|^2 = y_k^T y_k = x_k^T A^k (A^T)^k x_k = x_k^T x_k = \|x_k\|^2$, we have $\|y_k\| = \|x_k\|$. According to the triangle inequality $-\|y_{k+1} - y_k\| \le \|y_{k+1}\| - \|y_k\| \le \|y_{k+1} - y_k\|$, it holds that $|\|y_{k+1}\| - \|y_k\||^4 \le \|y_{k+1} - y_k\|^4$, which indicates that:

$$\begin{aligned} &|\zeta_{k+1} - \zeta_k|^4 \\ &= |\|y_{k+1}\| - \|y_k\||^4 \\ &\le \|y_{k+1} - y_k\|^4 \\ &= \left\| (A^T)^{k+1} [B_u u_{\max} + B_w w_k] \right\|^4 \\ &= \|B_u u_{\max} + B_w w_k\|^4 \\ &\le \left(\|B_u\|_2 \cdot \|u_{\max}\| + \|B_w\|_2 \cdot \|w_k\| \right)^4 \\ &\le \left(\|B_u\|_2 \cdot r_u + \|B_w\|_2 \cdot \|w_k\| \right)^4 \end{aligned} \tag{45}$$

Therefore, one obtains $\mathbb{E}\left\{ |\zeta_{k+1} - \zeta_k|^4 | \zeta_0, \ldots \zeta_k \right\} \le \mathbb{E}\left\{ \left(\|B_u\|_2 \cdot r_h + \|B_w\|_2 \cdot \|w_k\| \right)^4 \right\}$. Because of the boundedness of the fourth moment of $\|w_k\|$, it can be easily deduced that there exists a constant $M = M\left(\|B_u\|_2, r_h, \|B_w\|_2, C_4 \right) > 0$ such that $\mathbb{E}\left\{ \left(\|B_u\|_2 \cdot r_h + \|B_w\|_2 \cdot \|w_k\| \right)^4 \right\} \le M$, which yields the condition Eq. (41). Now all constants

$\{b, Z, M\}$ are well-defined. Note that x_0 implies $\zeta_0 = \|x_0\| < Z$. Therefore, in the light of Lemma 1, there exists a constant $\gamma = \gamma(b, Z, M) > 0$ such that $\sup_{k\in\mathbb{N}_0} \mathbb{E}\left\{\|x_k\|^2\right\} = \sup_{k\in\mathbb{N}_0} \mathbb{E}\left\{\zeta_k^2\right\} < \gamma$. This completes the proof. □

References

Allen, R. G. (1998). *Crop evapotranspiration : guidelines for computing crop water requirements (FAO irrigation and drainage paper, No. 56)*. Rome: Food and Agriculture Organization of the United Nations.

Bemporad, A., & Morari, M. (1999). Robust model predictive control: A survey. *Robustness in Identification and Control*, *245*, 207–226.

Ben-Hur, A., Horn, D., Siegelmann, H. T., & Vapnik, V. (2001). Support vector clustering. *Journal of Machine Learning Research*, *2*(Dec), 125–137.

Bertsimas, D., Gupta, V., & Kallus, N. (2018). Data-driven robust optimization. *Mathematical Programming*, *167*(2), 235–292.

Bertsimas, D., & Sim, M. (2004). The price of robustness. *Operations Research*, *52*(1), 35–53.

Bittelli, B., Campbell, G. S., & Tomei, F. (2015). *Soil physics with Python: Transport in the soil-plant-atmosphere system*. OUP Oxford.

Cai, J., Liu, Y., Lei, T., & Pereira, L. S. (2007). Estimating reference evapotranspiration with the FAO penman–Monteith equation using daily weather forecast messages. *Agricultural and Forest Meteorology*, *145*(1), 22–35.

Caldwell, M. M., Dawson, T. E., & Richards, J. H. (1998). Hydraulic lift: consequences of water efflux from the roots of plants. *Oecologia*, *113*(2), 151–161.

Campbell, G. S. (1988). Soil water potential measurement: An overview. *Irrigation Science*, *9*(4), 265–273.

Chatterjee, D., Hokayem, P., & Lygeros, J. (2011). Stochastic receding horizon control with bounded control inputs: A vector space approach. *IEEE Transactions on Automatic Control*, *56*(11), 2704–2710.

Chen, X., Sim, M., & Sun, P. (2007). A robust optmization perspective on stochastic programming. *Operations Research*, *55*(6), 1058–1071.

Choné, X., Van Leeuwen, C., Dubourdieu, D., & Gaudillère, J. P. (2001). Stem water potential is a sensitive indicator of grapevine water status. *Annals of Botany*, *87*(4), 477–483.

Delgoda, D., Malano, H., Saleem, S. K., & Halgamuge, M. N. (2016). Irrigation control based on model predictive control (MPC): formulation of theory and validation using weather forecast data and AQUACROP model. *Environmental Modelling & Software*, *78*, 40–53.

Flügge-Lotz, I. (1953). *Discontinuous automatic control*. Princeton University Press.

Fulton, A., Grant, J., Buchner, R., & Connell, J. (2014). *Using the pressure chamber for irrigation management in walnut, almond and prune*.

Gallego, A. J., Merello, G. M., Berenguel, M., & Camacho, E. F. (2019). Gain-scheduling model predictive control of a fresnel collector field. *Control Engineering Practice*, *82*, 1–13.

Galuppini, G., Magni, L., & Raimondo, D. M. (2018). Model predictive control of systems with deadzone and saturation. *Control Engineering Practice*, *78*, 56–64.

Gao, J., Ning, C., & You, F. (2019). Data-driven distributionally robust optimization of shale gas supply chains under uncertainty. *AIChE Journal*, *65*(3), 947–963.

Garcia, C. E., Prett, D. M., & Morari, M. (1989). Model predictive control: theory and practice—a survey. *Automatica*, *25*(3), 335–348.

Glenn, E. P., Huete, A. R., Nagler, P. L., Hirschboeck, K. K., & Brown, P. (2007). Integrating remote sensing and ground methods to estimate evapotranspiration. *Critical Reviews in Plant Sciences*, *26*(3), 139–168.

Gorissen, B. L., Yanıkoğlu, İ., & den Hertog, D. (2015). A practical guide to robust optimization. *Omega*, *53*, 124–137.

Goulart, P. J., Kerrigan, E. C., & Maciejowski, J. M. (2006). Optimization over state feedback policies for robust control with constraints. *Automatica*, *42*(4), 523–533.

Guo, Z. (2017). Daily variation law of solar radiation flux density incident on the horizontal surface. *Journal of Astrophysics & Aerospace Technology*, *8*.

Hargreaves, G. H., & Samani, Z. A. (1985). Reference crop evapotranspiration from temperature. *Applied engineering in agriculture*, *1*(2), 96–99.

Jones, H. G. (2013). *Plants and microclimate: A quantitative approach to environmental plant physiology* (3rd ed.). Cambridge University Press.

Kusiak, A., Li, M., & Zhang, Z. (2010). A data-driven approach for steam load prediction in buildings. *Applied Energy*, *87*(3), 925–933.

Kwon, W. H., & Han, S. H. (2006). *Receding horizon control: model predictive control for state models*. Springer Science & Business Media.

Leyffer, S., Menickelly, M., Munson, T., Vanaret, C., & Wild, S. M. (2020). A survey of nonlinear robust optimization. *INFOR: Information Systems and Operational Research*, *58*(2), 342–373.

Lofberg, J. (2004). YALMIP : a toolbox for modeling and optimization in MATLAB. In *2004 IEEE international conference on robotics and automation* (pp. 284–289).

Lozoya, C. (2014). Model predictive control for closed-loop irrigation. *IFAC Proceedings Volumes*, *47*(3), 4429–4434.

Marquis, P., & Broustail, J. P. (1988). SMOC, a bridge between state space and model predictive controllers: application to the automation of a hydrotreating unit. *IFAC Proceedings Volumes*, *21*(4), 37–45.

Mattingley, J., Wang, Y., & Boyd, S. (2011). Receding horizon control. *IEEE Control Systems Magazine*, *31*(3), 52–65.

McCarthy, A. C., Hancock, N. H., & Raine, S. R. (2014). Simulation of irrigation control strategies for cotton using Model Predictive Control within the VARIwise simulation framework. *Computers and Electronics in Agriculture*, *101*, 135–147.

Mccutchan, H., & Shackel, K. A. (1992). Stem-water potential as a sensitive indicator of water-stress in prune trees (Prunus domestica L. cv. French). *Journal of the American Society for Horticultural Science*, *117*(4), 607–611.

Meteogram Generator (0000). Dept of Geological and Atmospheric Sciences, Iowa State University. [Online]. Available: https://www.meteor.iastate.edu/ckarsten/bufkit/image_loader.phtml.

Moro, S., Cortez, P., & Rita, P. (2014). A data-driven approach to predict the success of bank telemarketing. *Decision Support Systems*, *62*, 22–31.

Ning, C., & You, F. (2017). Data-driven adaptive nested robust optimization: General modeling framework and efficient computational algorithm for decision making under uncertainty. *AIChE Journal*, *63*(9), 3790–3817.

Ning, C., & You, F. (2018a). Data-driven decision making under uncertainty integrating robust optimization with principal component analysis and kernel smoothing methods. *Computers & Chemical Engineering*, *112*, 190–210.

Ning, C., & You, F. (2018b). Data-driven stochastic robust optimization: General computational framework and algorithm leveraging machine learning for optimization under uncertainty in the big data era. *Computers & Chemical Engineering*, *111*, 115–133.

Ning, C., & You, F. (2019). Data-driven wasserstein distributionally robust optimization for biomass with agricultural waste-to-energy network design under uncertainty. *Applied Energy*, *255*, Article 113857.

Oosterhuis, D. M. (1987). A technique to measure the components of root water potential using screen-caged thermocouple psychrometers. *Plant and Soil*, *103*(2), 285–288.

Pagay, V., et al. (2014). A microtensiometer capable of measuring water potentials below -10 MPa. *Lab on a Chip*, *14*(15), 2806–2817.

Paulson, J. A., Buehler, E. A., Braatz, R. D., & Mesbah, A. (2020). Stochastic model predictive control with joint chance constraints. *International Journal of Control*, *93*(1), 126–139.

Pemantle, R., & Rosenthal, J. S. (1999). Moment conditions for a sequence with negative drift to be uniformly bounded in Lr. *Stochastic Processes and their Applications*, *82*(1), 143–155.

Perez, T., Tzeng, C.-Y., & Goodwin, G. C. (2000). Model predictive rudder roll stabilization control for ships. *IFAC Proceedings Volumes*, *33*(21), 45–50.

Pidsley, R., Wong, C. C. Y., Volta, M., Lunnon, K., Mill, J., & Schalkwyk, L. C. (2013). A data-driven approach to preprocessing illumina 450k methylation array data. *BMC Genomics*, *14*(1), 293.

Qin, S. J., & Badgwell, T. A. (2003). A survey of industrial model predictive control technology. *Control Engineering Practice*, *11*(7), 733–764.

Romero, R., Muriel, J. L., García, I., & Muñoz de la Peña, D. (2012). Research on automatic irrigation control: State of the art and recent results. *Agricultural Water Management*, *114*, 59–66.

Shang, C., Chen, W.-H., Stroock, A. D., & You, F. (2019). Robust model predictive control of irrigation systems with active uncertainty learning and data analytics. *IEEE Transactions on Control Systems Technology*, 1–12.

Shang, C., Huang, X., & You, F. (2017). Data-driven robust optimization based on kernel learning. *Computers & Chemical Engineering*, *106*, 464–479.

Shang, C., & You, F. (2019). Data analytics and machine learning for smart process manufacturing: Recent advances and perspectives in the big data era. *Engineering*, *5*(6), 1010–1016.

Shen, D., Lim, C.-C., & Shi, P. (2020). Robust fuzzy model predictive control for energy management systems in fuel cell vehicles. *Control Engineering Practice*, *98*, Article 104364.

Sturzenegger, D., Gyalistras, D., Morari, M., & Smith, R. S. (2016). Model predictive climate control of a swiss office building: Implementation, results, and cost–benefit analysis. *IEEE Transactions on Control Systems Technology*, *24*(1), 1–12.

Sumner, D. M., & Jacobs, J. M. (2005). Utility of penman–Monteith, priestley–taylor, reference evapotranspiration, and pan evaporation methods to estimate pasture evapotranspiration. *Journal of Hydrology*, *308*(1), 81–104.

United Nations World Water Assessment Programme (2018). *The United Nations world water development report 2018: Nature-based solutions for water*. UNESCO Paris.

Vörösmarty, C. J., Green, P., Salisbury, J., & Lammers, R. B. (2000). Global water resources: vulnerability from climate change and population growth. *Science*, *289*(5477), 284–288.

Weizmann, A., Görges, D., & Lin, X. (2018). Energy-optimal adaptive cruise control combining model predictive control and dynamic programming. *Control Engineering Practice*, *72*, 125–137.

Xi, Y.-G., Li, D.-W., & Lin, S. (2013). Model predictive control — status and challenges. *Acta Automatica Sinica*, *39*(3), 222–236.

Yuan, Y., Li, Z., & Huang, B. (2018). Nonlinear robust optimization for process design. *AIChE Journal*, *64*(2), 481–494.

Zhang, Y., Jin, X., Feng, Y., & Rong, G. (2018). Reprint of: Data-driven robust optimization under correlated uncertainty: A case study of production scheduling in ethylene plant. *Computers & Chemical Engineering*, *116*, 17–36.

Zhu, S. (2020). *Development of Sensing Framework for the Soil-Plant-Atmosphere Continuum* (Ph.D dissertation), Ithaca: Cornell University.